Research Article | Vol. 29, No. 15 / 19 July 2021 / Optics Express 23569
Optics EXPRESS

Thermo-optic tuning of a nematic liquid crystal-filled capillary whispering gallery mode resonator

ZHE WANG,[1,*] ARUN KUMAR MALLIK,[1] FANGFANG WEI,[1] ZHUOCHEN WANG,[1] ANURADHA ROUT,[1] QIANG WU,[2] AND YULIYA SEMENOVA[1]

[1]*Photonics Research Centre, School of Electrical and Electronic Engineering, Technological University Dublin, Dublin 7, Ireland*
[2]*Department of Mathematics, Physics and Electrical Engineering, Northumbria University, Newcastle Upon Tyne NE1 8ST, UK*
[*]*D19125415@mytudublin.ie*

Abstract: A novel tunable whispering gallery modes (WGMs) resonator based on a nematic liquid crystal (LC)-filled capillary and magnetic nanoparticles (MNPs)-coated tapered fiber has been proposed and experimentally demonstrated. Thermo-optic tuning of the WGM resonances has been demonstrated by varying optical pump laser power injected into the MNPs-coated fiber half-taper inside the capillary. The tuning mechanism relies on the change of the effective refractive index (RI) of the nematic LC, caused by the photo-thermal effect of MNPs on the surface of the fiber half-taper inducing a temperature change inside the capillary. Tuning of the WGM resonances with sensitivities of 101.5 ± 3.5 pm/mW and 146.5 ± 3.5 pm/mW and tuning ranges of 1.96 nm and 3.28 nm respectively for the two types of liquid crystals (MLC-7012, MDA-05-2782) has been demonstrated. In addition, the relationship between the optical power of the pump laser and the local temperature of the nematic LC was investigated and the heating rate is estimated as 1.49 °C/mW. The proposed thermo-optic tuning scheme has many potential applications in tunable photonic devices and sensors.

1. Introduction

Whispering gallery modes (WGMs) resonance phenomenon occurs when light is trapped within a circular dielectric structure by total internal reflections at the interface between a higher refractive index (RI) dielectric resonator and a lower RI surrounding medium [1,2]. Light from an optical source can be launched into such a resonator by evanescent coupling using a prism or a tapered optical fiber. Only the specific light wavelengths that meet the phase condition become trapped within the resonator, while all other wavelengths continue to propagate in the adjacent output fiber taper. As a result, the transmission spectrum of the tapered fiber contains multiple dips with high quality factors (Q). Any changes in the resonator size or in the effective RI will lead to spectral shifts in the resonant wavelength dips observed in the transmission spectrum.

Owing to the advantages of small mode volumes and high Q factors, in the last few decades WGM resonators have been investigated extensively both theoretically and experimentally for various applications including nonlinear optics [3], microcavity lasers [4], optical signal processing [5] and optical sensing [6]. Recent progress in micro- and nano-fabrication technologies reduced the cost and increased feasibility of fabrication of WGM resonators with the dimensions in the order of micrometers or smaller [7]. Operating principle of WGM resonator-based sensors relies on the measurement of the spectral shift of the resonant modes that can be related to the measurand of interest. Owing to the high Q factors of the resonant modes, WGM sensors typically offer high measurement resolution and sensitivity, making them particularly attractive

#432103 https://doi.org/10.1364/OE.432103
Journal © 2021 Received 24 May 2021; revised 23 Jun 2021; accepted 24 Jun 2021; published 9 Jul 2021

Optics EXPRESS

for biosensing applications. A number of WGM sensors have been reported for virus [8], nucleic acid [9] and protein [10] detection with detection limits down to a single-molecule level opening new prospects for the next-generation clinical diagnostics.

To fully explore the advantages of WGMs, a variety of resonator geometries that support WGMs have been proposed and developed including the microsphere [11], microcapillary [12], microcylinder [13], microring [14] and microbottle resonators [15]. In particular, the microcapillary- based WGM resonators, also known as optofluidic ring resonators (OFRR), have attracted growing attention due to the possibility of their integration with microfluidic platforms. For example, an optically tunable OFRR integrated with magnetic fluids with a high tuning sensitivity of 0.15 nm/mW and a tuning range of 3.3 nm has been reported in [16]. Another optical tunning scheme based on the magnetic-fluid-infiltrated microstructured optical fibers was experimentally demonstrated with a sensitivity of 0.034 nm/mW in [17]. It should be noted that the above-mentioned tunable resonators suffer from poor uniformity of the magnetic fluids due to sedimentation of magnetic nanoparticles within the capillary or fiber cavity. In addition, the water based magnetic fluids dry out quickly and thus require immediate sealing off these containers. The above disadvantages could limit the applications of such magnetic-fluid- based tunable resonators in practical devices.

Liquid crystals (LCs), due to their high birefringence and high thermo- & electro-optic coefficients, have become popular materials in a wide range of optical devices, such as liquid crystal displays [18], tunable filters [19], switches [20], lasers [21] and spatial light modulators [22]. Several studies focused on investigation of LC droplet microresonators where tuning was achieved by changing environmental temperature or applied electric field intensity for temperature and magnetic field sensing [23,24]. It should be noted however that the lack of stability in terms of the droplets shape under the influence of environmental perturbations may result in measurement errors for the above sensors.

In this study we propose and experimentally demonstrate a novel tunable WGM capillary resonator filled with a nematic LC, where thermo-optical tuning is realized using a pump laser radiation injected into a fiber half-taper coated with a layer of magnetic nanoparticles (MNPs). The proposed scheme allows to overcome the above issues associated with sedimentation and lack of stability. Thermo-optical tuning relies on the conversion of pump laser radiation into heat by the MNPs resulting in the increase of temperature of the nematic LC inside the capillary. This in turn causes the change of the effective RI of the liquid crystal and the corresponding spectral shift of the WGM resonances. Two types of commercially available nematic liquid crystals (MLC-7012, MDA-05-2782) are employed to investigate the proposed tuning mechanism with the demonstrated tuning ranges of 1.96 nm and 3.28 nm and sensitivities of 101.5 ± 3.5 pm/mW and 146.5 ± 3.5 pm/mW, respectively. For comparison and in order to demonstrate the effect of MNPs on the tunability, the proposed scheme was characterized utilizing an uncoated fiber half-taper. The result shows that the sensitivities of the corresponding WGM resonators infiltrated with the nematic LCs in the absence of MNPs on the surface of the half-taper are approximately 8 and 43 times lower than those with MNP of MLC-7012 and MDA-05-2782 respectively. To the best of our knowledge, this is the first attempt to utilize the photothermal effect of the MNPs coating to realize an effective thermo-optical tuning of a WGM capillary resonator with good stability. The proposed scheme shows excellent potential for applications in optical tunable filters, switches and sensors.

2. Experimental setup and sample preparation

2.1. Fiber half-taper fabrication and coating

A standard single-mode telecommunications fiber (SMF-28 from Corning) with the core and cladding diameters of 8.3 μm and 125 μm was used to fabricate the tapered fiber. In our experiment, a 3 cm length of protecting polymer coating was stripped off at the center of a 1 m

Optics EXPRESS

long SMF-28 fiber section. The diameter of the stripped fiber section was then reduced down to 10 µm using the customized microheater brushing technique [25]. To realize that, the stripped fiber was fed through a slit in a ceramic microheater where the temperature was approximately 1300 °C and the two fiber ends were fixed to the computer controlled translational stages. The customized computer program realized simultaneous side-to-side and stretching motion of the fiber within the microheater slit in order to reach the set taper waist diameter. The fabricated full fiber taper then was cut in the middle of the uniform waist to form two half-tapers.

The half-tapers then were coated with MNPs by dipping into a solution with a high concentration (10 mg/ml) of magnetic nanoparticles (Micromod Partikeltechnologie GmbH, nanomag@-D, 09-20-132). Prior to the coating, the MNPs solution was treated in an ultrasonic bath for 10 minutes to ensure its uniformity. The fabricated half-tapers then were dipped into the MNPs solution and pulled out at a rate of 0.5 mm/s. Scanning electron microscope (SEM) imaging showed that a faster pulling rate resulted in a larger amount of MNPs deposited on the half-tapers surfaces. The coated half-tapers then were cured at room temperature for 48 hours. Figure 1(a) shows an SEM image of a coated taper end whose diameter is estimated as 12.2 µm. Figures 1(b) and 1(c) are SEM images illustrating the MNPs layer thickness and distribution of the MNPs on the surface of the fiber. It can be seen from the images that the coating thickness is approximately 99.2 nm. Due to the observed clustering of MNPs on the surface of the fiber (Fig. 1(c)) the average diameter of MNPs was only approximately estimated as ~85 nm.

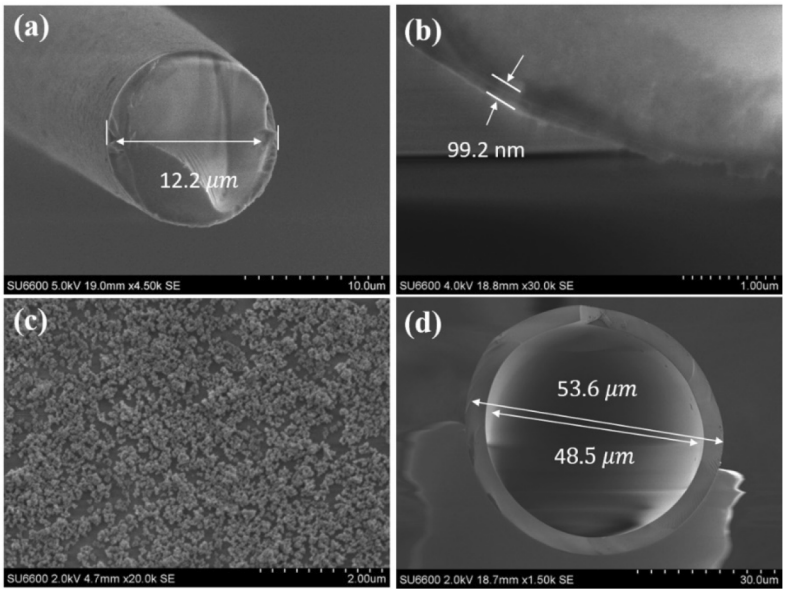

Fig. 1. SEM images of the fiber half-taper coated with MNPs and the stretched capillary: (a, b) fiber end view, (c) side view, (d) capillary end view.

2.2. *Fabrication of the WGM capillary resonator*

A thin-walled WGM cylindrical resonator was prepared by heating and stretching a silica capillary (Polymicro Technology) with the outer diameter of 850 µm and inner diameter of 700 µm using the ceramic microheater based set-up described in the previous section. As shown in Fig. 1(d), the capillary diameter after tapering was 53.6 µm and the wall thickness was 2.55 µm. Subsequently, the capillary was fixed on a glass slide at a height of 10 mm from its surface using two drops of a UV curable epoxy.

Optics EXPRESS

The next fabrication step involved light coupling into the capillary resonator fixed on a glass slide using a tapered fiber. Another full fiber taper with the uniform waist diameter of 1 μm for light coupling into the resonator was fabricated using the microheater setup. The input and output of the tapered fiber were connected to a broadband light source (Thorlabs, 1500–1600 nm) through a polarization controller and an optical spectrum analyzer (OSA, Advantest, Q8384), respectively. A micro-translation stage was used to place the uniform taper waist in close proximity and perpendicularly to the capillary to facilitate the most efficient light coupling. Once the physical contact between the capillary and the tapered fiber was achieved, the fiber taper transmission spectrum with WGM dips was observed at the OSA screen. The coupling efficiency was then further improved by adjusting the position of the fiber taper with respect to the capillary using the micro-translation stage and visually monitoring the quality of the transmission spectrum using the OSA. The extinction ratio of the WGM spectrum was further improved by adjusting the input light polarization by means of polarization controller. After achieving the transmission spectrum with the highest possible Q factor, the micro-translation stage was adjusted to maintain tight contact between the capillary and the tapered fiber. Finally, both ends of the full fiber taper were fixed on a glass slide with UV curable epoxy for better mechanical stability.

2.3. Fabrication of the WGM capillary resonator

At the next step the WGM micro-capillaries were infiltrated with nematic LCs, MLC-7012 (n_e=1.5304, n_o=1.4644, measured at 589.3 nm and 20 °C, clearing point: 91°C) and MDA-05-2782 (n_e=1.6152, n_o=1.4912, measured at 589.3 nm and 20 °C, clearing point:106°C) (Licristal, Merck). Two 2 cm long capillaries were firstly filled with the respective nematic LCs at room temperature using a syringe and a pump at one of the capillary ends. Following the infiltration each capillary was visually inspected to ensure the absence of air bubbles. Then the alignment of the LC molecules in the capillaries was studied by placing them between crossed polarizers under a microscope, as illustrated in Fig. 2(d). The polarization micrographs for the case of MDA-05-2782 filled capillary and the corresponding interpretation of the LC molecules alignment inside the capillary are presented in Figs. 2(a-c). In Fig. 2(a) the direction of the capillary axis coincides with the direction of input polarizer (0°). Images (b) and (c) correspond to the rotation of the capillary by 22.5° and 45° with respect to the input polarizer axis. The light extinction phenomenon evident from the micrographs indicates that at the center of the capillary optical axis of the LC molecules (nematic director) lies in plane of the capillary axis. In all three images (a-c) the dark areas within the capillary correspond to those areas where the alignment of the LC director is either perpendicular or parallel to the input polarizer. When the LC director is oriented in plane of the capillary axis but with an azimuthal orientation that lies between the polarizer and analyzer, the light transmitted through the LC gains an elliptical polarization leading to a bright optical appearance of the LC. It can also be concluded from all three cases of the capillary orientation that the LC director in the center of the capillary is aligned closely with the capillary axis, while it exhibits “splayed” alignment towards the cylinder walls. At the surface of the capillary wall the LC molecules are aligned along the surface of the wall and perpendicularly to the capillary axis, as indicated by the darker appearance close to the capillary walls.

Next the fiber half-tapers coated with MNPs were inserted in each of the LC-infiltrated capillary resonators (shown in Fig. 2(a)) as follows. Both the capillary and the coated tapered fiber were separately fixed on two micro-translation stages. By precisely controlling the position of the two stages, the MNPs coated tip of the half-taper was gradually inserted in the LC-filled capillary. The position of the fiber tip within the capillary was adjusted so that it was located close to the coupling point (outside the capillary). Once the desired position of the half-taper tip was reached, it was fixed on the glass slide using a UV curable epoxy. The second sample of the WGM resonator infiltrated with MLC-7012 was fabricated using the same sequence of steps.

Optics EXPRESS

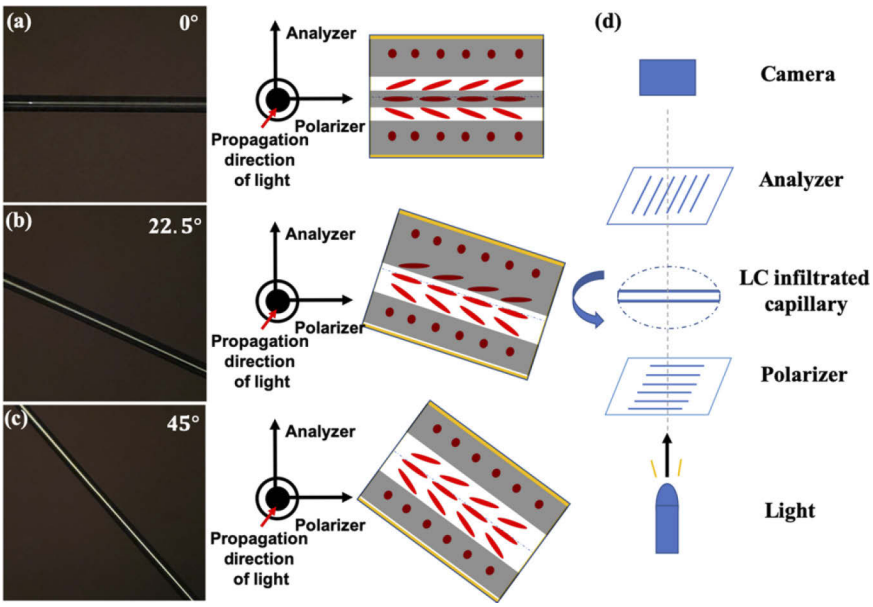

Fig. 2. Polarization micrographs of a cylindrical WGM resonator infiltrated with MDA-05-2782 and corresponding alignment of the LC molecules in the capillary: (a) 0° angle between the capillary axis and input polarizer, (b) capillary rotated by 22.5° and (c) by 45° with respect to input polarizer; (d) schematic of the setup for investigation of the LC alignment.

Figure 3(a) shows experimentally measured transmission spectra for a fiber taper coupled to the capillary WGM resonator before, after its infiltration with MDA-05-2782 and after inserting the MNPs coated tapered fiber into the infiltrated capillary. As one can see from the figure, after the infiltration of the capillary with the LC the WGM spectral dips in the transmission spectrum of the full taper shifts towards longer wavelengths compared to the initial spectrum of an air-filled capillary. In addition, the spectrum after infiltrating it with MDA-05-2782 has many sidelobes and noise, which could be explained by the birefringence of the LC [7]. The Q-factors for the capillary WGM resonator before, after its infiltration with MDA-05-2782 and after inserting the MNPs coated tapered fiber into the infiltrated capillary were estimated from the experimental spectra by measuring the full width at half maximum (FWHM) of the WGM resonance near 1544 nm at room temperature (17°C). The corresponding values of the Q-factor were calculated as 2.29×10^3, 2.08×10^3, and 2.14×10^3 respectively. The relatively stable Q-factors indicate the stability of the nematic LC inside capillary and that the alignment of the nematic LC doesn't change with inserting the MNPs coated tapered fiber into the infiltrated capillary.

The spectral shifts of the WGM resonances in Fig. 3(a) can be explained by analyzing the approximate expression for the resonant wavelength λ_l (where l represents the angular mode number) in a layered cylindrical capillary WGM resonator [26]:

$$\lambda_l \approx \frac{2\pi a}{l}(f_1 n_1 + f_2 n_2 + f_3 n_3) \tag{1}$$

where a is the outer radius of the WGM resonator, n_1, n_2, and n_3 are the RIs of the capillary core material, silica capillary wall and the surrounding air, respectively and f_1, f_2 and f_3 are corresponding fractions of the mode energy in each layer.

To analyze the changes in the fractional mode distributions, considering only the fundamental TE mode for simplicity, in accordance with radial TE filed equations for the cylindrical WGM

Optics EXPRESS

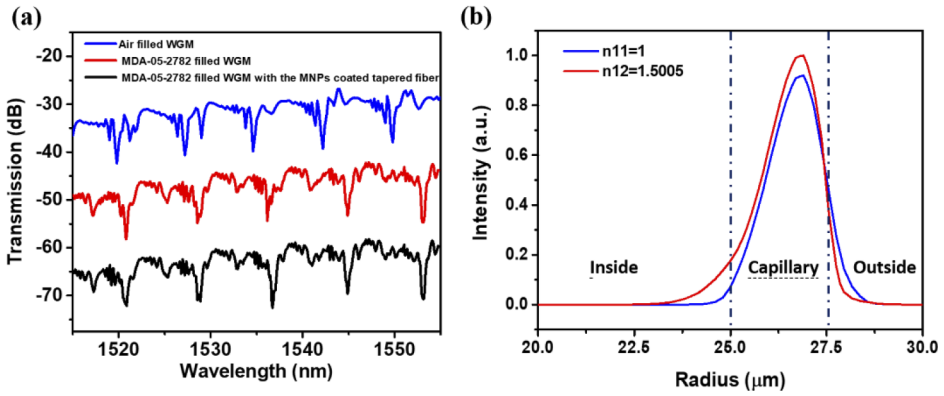

Fig. 3. (a) WGM spectra of the same capillary resonator: empty (blue line), filled with MDA-05-2782 (red line) and filled with MDA-05-2782 and with inserted MNPs coated tapered fiber (black line), (b) simulated TE-polarized electric field intensity $|E(r)|^2$ for different values of the capillary core RIs.

resonator, we have [26]:

$$E(r) = \begin{cases} A_l J_l(n_1 kr), & r \le b \\ B_l H_l^{(2)}(n_2 kr) + H_l^{(1)}(n_2 kr), & b < r \le a \\ D_l H_l^{(1)}(n_3 kr), & r > a \end{cases} \quad (2)$$

where r is the radial direction of capillary, a and b are the outer and inner radii of capillary, J_l is the first kind of cylindrical Bessel function with order l, $H_l^{(1)}$ and $H_l^{(2)}$ are cylindrical Hankel functions with order l, k is the vacuum wavevector, A_l, B_l, and D_l are constants. Using Eq. (2), the electric field intensity $|E(r)|^2$ distribution has been simulated and shown in Fig. 3(b) for the fundamental mode with $l = 152$ in a capillary with an outer radius $a = 27.6\,\mu$m, inner radius $b = 25\,\mu$m, $n_2 = 1.444$, $n_3 = 1$ for two values of the core material RI: $n_{11} = 1$ (air-filled), $n_{12} = 1.5005$ (filled with MDA-05-2782). Given the complex alignment of LC molecules in the capillary, an average value of RI for MDA-05-2782 was adopted to analyze the fractional mode distributions ($n_{12} = n_{average} = (n_e + 2n_o)/3$). To take account of dispersion, the values of n_e and n_o for MDA-05-2782 at 1550 nm were approximately estimated as 1.5769 and 1.4623 using the three-coefficient Cauchy model [27]. As can be seen from Fig. 3(b), the electric field intensity $|E(r)|^2$ near the boundary between the core material and the inner capillary wall increases with the increase of n_1, while that close to the boundary of the outside capillary wall with air decreases. The fractions of mode energy f_1, f_2 and f_3 can be calculated as 0.02%, 98%, and 1.98% respectively for the n_{11}=1 case, 0.75%, 98.5% and 0.75% respectively for the n_{12}=1.5005 case. The simulation result demonstrates that an increase in the n_1 leads to an increase of the mode fractions f_1 and f_2 with a decrease of the mode fraction f_3, wich also contributes to the red shift of λ_l according to Eq. (1). Therefore both, the increase in the refractive index of the capillary core material and increases in the mode energy fractions within the capillary core and wall are consistent with the experimentally observed red shift in Fig. 3(a). It should be noted that the spectrum of the resonator after inserting MNPs coated tapered fiber remains almost unchanged as the RI change resulted from inserting the half-taper in the middle of the capillary only affects the higher order WGM modes.

Optics EXPRESS

3. Experimental results and discussion

The schematic of the experimental setup for characterization of the tunable WGM resonators is shown in Fig. 4. A 980 nm laser source (Superlum, Pilot-6) used as an optical pump was connected to the free end of the MNPs coated half-taper and an optical power meter (dBm Optics, Model 4100) using an optical splitter with a power ratio of 86.7%/13.3% measured @980 nm. The WGM resonances were observed by the OSA in the transmission spectrum of the full fiber taper optically coupled to the capillary and connected to the broadband optical source through the polarization controller, as described in the previous section.

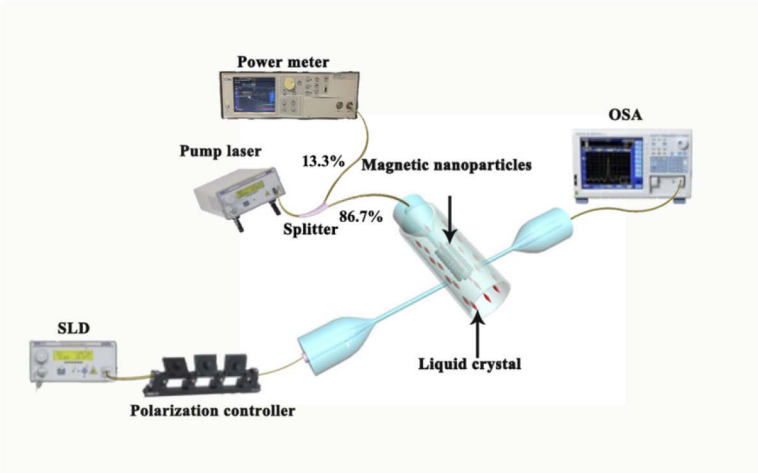

Fig. 4. Schematic diagram of the LC-infiltrated capillary WGM resonator and experimental setup for its characterization.

To study the optical tunning of the WGMs, a series of experiments were carried out by increasing the pump laser power launched into the MNPs coated fiber half-taper from 0 to 23.4 mW with a step of 2.6 mW, and then decreasing the optical power with the same step back to 0. To realize this, a customized LabVIEW PC program was used to control the laser source power and to record the transmission OSA spectra of the coupling fiber taper with time intervals of 30 s (determined by the speed of the OSA in a high-resolution mode). Each series of data was taken after an 8-minute interval to allow for the heat distribution. Every data point was determined as the average of 5 collected data (collected between the 6th and 8th minute of each cycle) to reduce the errors. The entire experimental setup was placed in a thermally insulated chamber to minimize external temperature perturbations.

The transmission spectra of the coupling tapered fiber for the WGM resonators infiltrated with MLC-7012 (MLC) and MDA-05-2782 (MDA) at different levels of the pump laser power are shown in Figs. 5(a) and (b) respectively. As can be seen from the graphs, both the MLC and MDA spectra experience blue shift with the increase of the pump laser power. A decrease of the pump laser power results in a gradual red shift of the spectra and return back to their initial positions at zero pump power, demonstrating good tuning capabilities and reversibility of the proposed scheme. It should be noted that the shapes of spectra don't change significantly with the increase of the pump power, indicating good stability of the MNPs coating on the surface of the tapered fiber.

Figures 6(a) and (b) summarize the dependences of the selected WGM dips versus the pump laser power. As one can see from the graphs the resonant dips (at circa 1583.04 nm for MLC-WGM and at circa 1558.48 nm for MDA-WGM) show liner dependencies with both increase and decrease of the pump power. The maximum tuning ranges for the two samples are 1.96 nm and 3.28 nm,

Optics EXPRESS

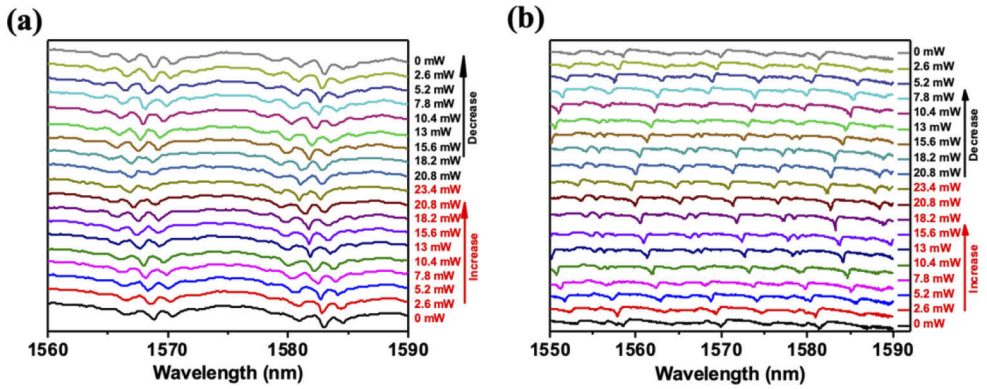

Fig. 5. Transmission spectra of the coupling fiber taper for WGM resonators infiltrated with (a) MLC-7012 and (b) MDA-05-2782 at different values of laser power launched into the capillary through the half-taper.

respectively in the range of pump powers from 0 to 23.4 mW. For the MLC-WGM sample, the linear fitting equation for power increase is y= -0.098x+1583.057, with a correlation coefficient of 0.984, and the corresponding linear fit equation for the power decrease is y= −0.105x+1583.22, with a correlation coefficient of 0.979. Considering the uncertainty of calculations of 3.5 pm/mW, the sensitivity of the dip to pump power achieved in the experiment for MLC-WGM is 101.5 ± 3.5 pm/mW. Likewise, the linear fitting dependencies for MDA-WGM are y= −0.15x+1558.223 and y= −0.143x+1558.259, with the sensitivity to pump power of 146.5 ± 3.5 pm/mW. It should be noted that the differences between the tunable range and sensitivities between MLC-WGM and MDA-WGM samples illustrated in Figs. 6(a) and (b) are likely due to the differences in the LC materials properties, such as RI values and their temperature dependencies. In order to evaluate the stability and repeatability of the proposed device, the initial experiments were repeated 5 days after the initial ones. The corresponding data showed less than 5% difference in sensitivities to pump power for both samples, confirming good stability and repeatability of performance

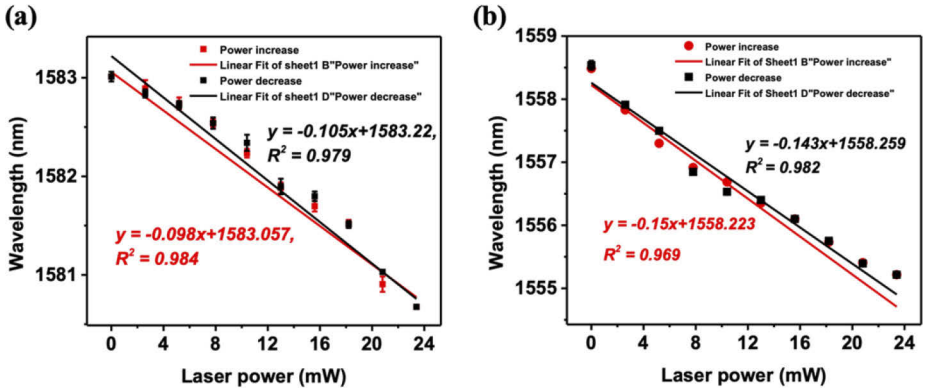

Fig. 6. Experimental data and linear fitting of the selected spectral dips versus pump power for (a) MMLC-WGM and (b) MMDA-WGM on heating (red) and cooling (black).

The observed optical tuning effect in the proposed WGM resonator system can be explained by the thermo-optic response of the nematic LCs. More specifically, when we the pump laser power supplied through the half-taper increases, the MNPs on its end surface absorb the radiation heating up the surrounding nematic LC. This leads to a decrease of the effective RI and birefringence of

Optics EXPRESS

the nematic LC. The temperature induced wavelength shift can be described using the following equation [28]:

$$\Delta\lambda = \lambda\left(\alpha\Delta T + \frac{1}{n_{core}}\frac{dn_{core}}{dT}\Delta T + \frac{1}{n_{wall}}\frac{dn_{wall}}{dT}\Delta T\right) \tag{3}$$

where α is the thermal expansion coefficient of the cylindrical WGM resonator, $\frac{dn_{core}}{dT}$ and $\frac{dn_{wall}}{dT}$ are the thermo-optic coefficients of the nematic LC and the silica capillary, n_{core} and n_{wall} n are the effective RIs of the nematic LC and silica capillary, respectively. ΔT is the change in temperature resulting from the absorption of the pump radiation by the MNPs and thermal energy transfer to the surrounding LC, which is determined by the absorption coefficient of the MNPs at the pump laser wavelength, pump laser power, as well as the efficiency of the heat transfer between the MNPs and nematic LC. For a nematic LC-infiltrated capillary, the thermal expansion includes the thermal expansion of the silica capillary and the nematic LC. However, in both cases the induced $\Delta\lambda$ can be neglected as the thermal expansion coefficients of both silica and LC are negligibly small (in the order of 10^{-6} K^{-1} [29] for silica). Considering the small thermo-optic coefficient of the silica capillary ($\sim 10^{-5}$ K^{-1}) [29], $\lambda\frac{1}{n_{core}}\frac{dn_{core}}{dT}\Delta T$ is likely the main factor determining the $\Delta\lambda$. Therefore, for a specific laser wavelength and LC material, pump laser power is the main factor determining the $\Delta\lambda$. Given the negative thermo-optic coefficient of the LC [30], the WGM resonant wavelengths experience linear blue-shift with the increase in temperature (pump power) which is in agreement with the experimental data in Fig. 6.

To better understand the demonstrated WGM tuning mechanism and in an attempt to establish a relationship between the optical power of the pump laser and the local temperature of the nematic LC, temperature response of the MDA-WGM sample was characterized at different temperatures in the absence of pump radiation. In this experiment, the WGM resonator was placed on a hot stage to control its temperature in the range from 17 °C to 60 °C at intervals of 5 °C. Figure 7(a) illustrates the transmission spectra of the MDA-WGM at different temperatures. As expected, the dips in the MDA-WGM spectrum experience blue shift with the increase in temperature, demonstrating similar tendency with the results obtained using pump laser radiation. As is shown in Fig. 7(b), linear fitting of the wavelength response data indicates sensitivity of 98 pm/°C with a linear regression coefficient of 0.98.

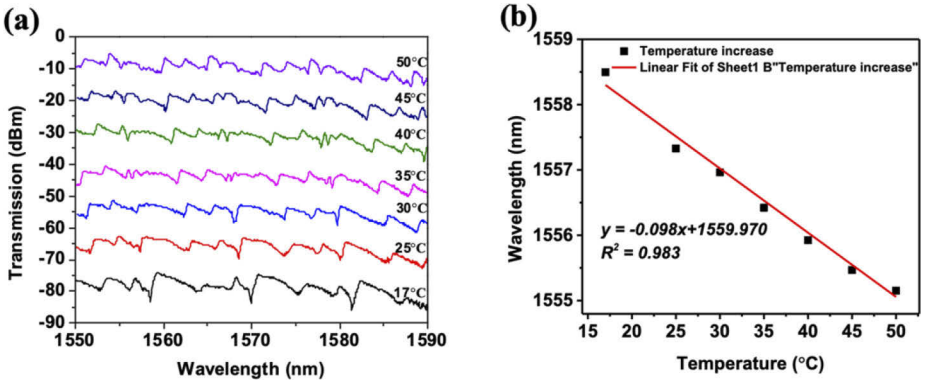

Fig. 7. (a) Transmission spectra of MMDA-WGM at different temperatures; (b) Linear fitting of the spectral shift data versus temperature for MMDA-WGM.

Based on the two experiments described above, it is possible to roughly estimate the increase in the WGM capillary temperature in the vicinity of the taper end per unit of pump laser power increase as 1.49 °C/mW. This calculation is carried out based on the data for the spectral dip near 1558.5 nm. In order to establish the influence of the MNPs coating on the tuning properties of the proposed WGM capillary resonator, similar experiments were carried out with uncoated

Optics EXPRESS

half-tapers. To realize this, two uncoated tapered fibers were inserted into the MLC-7012 and MDA-05-2782 infiltrated capillaries respectively to implement the WGM tuning scheme while maintaining the same fabrication and experimental procedures as in the previously described experiments. Figures 8(a) and (c) show the corresponding spectral responses of the MLC-WGM and MDA-WGM resonators at different values of pump laser power in the range from 0 to 20.8 mW with 5.2 mW intervals. Figures 8(b) and (d) show the corresponding experimental data and linear fittings for the selected spectral dips at circa 1547.85 nm and 1498.75 nm as a function of laser power, respectively. As can be seen from Figs. 8(b) and (d), while the dependencies are linear, as in the previous experiments, the resonance dips shift merely by 0.26 nm and 0.08 nm in the same pump power range, resulting in sensitivities of 13 pm/mW and 3.5 pm/mW, respectively. These sensitivities are 8 times (for the MLC-WGM) and 43 times (for the MDA-WGM) smaller compared to those obtained in the previous experiments with MNPs-coated tapered fibers. This further confirms the importance of the MNPs coating for an efficient heat transfer from the pump laser source to the LC, filling the capillary resonators.

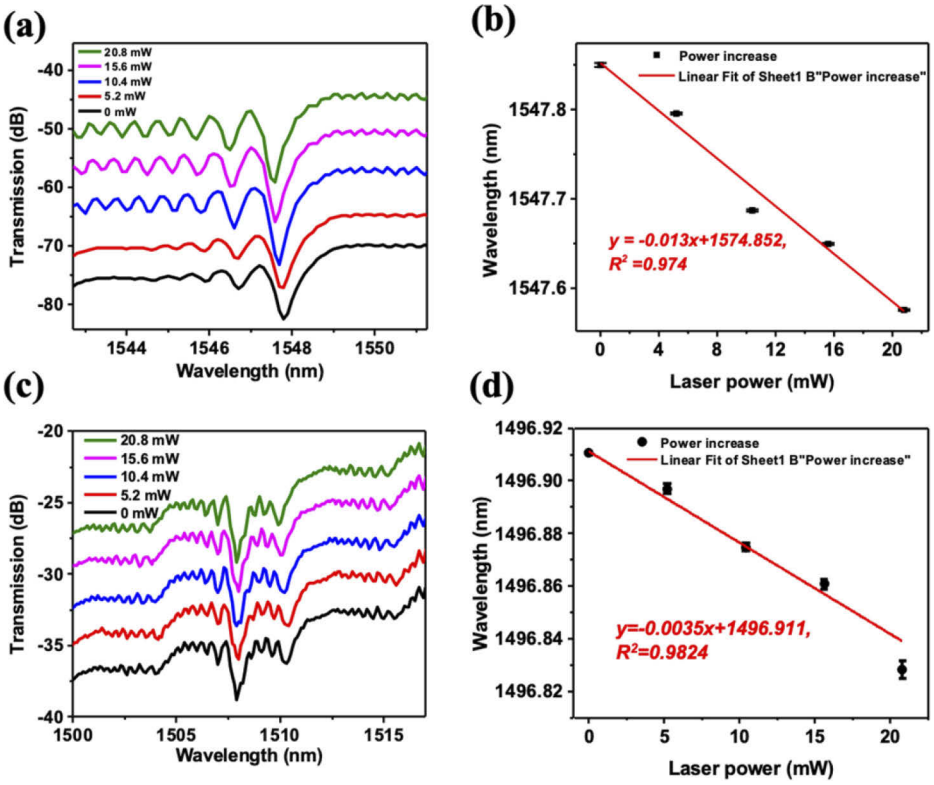

Fig. 8. (a) Transmission spectra of MLC-WGM at different pump laser powers; (b) linear fitting of the spectral shift data in (a) for a selected dip; (c) transmission spectra of MDA-WGM at different pump laser powers; (d) linear fitting of the spectral shift data in (c) for a selected dip.

In order to evaluate the response time of the proposed thermo-optic tuning system, another experiment was carried out where the OSA in the previous setup was replaced by a photo-detector (Thorlabs, PDA10CS-EC) connected with an oscilloscope (Keysight, MSO-X 2022A). The response time was defined as the time period when the signal at the photo-detector increases from 10% to 90% of its maximum value [31]. The recorded voltage from the photo-detector versus time dependence is shown in Fig. 9. The abrupt voltage changes from 89.75 mV to 91.6 mV occurred

Optics EXPRESS

when the input laser was turned on and off around the 8th and 396th seconds from the start of the experiment. The corresponding reaction and relaxation times are approximately 700 and 200 ms respectively. Such response times in the order of hundreds milliseconds indicate that the proposed thermo-optic tuning WGMs resonator is suitable for applications in the low-frequency photonic devices and sensors.

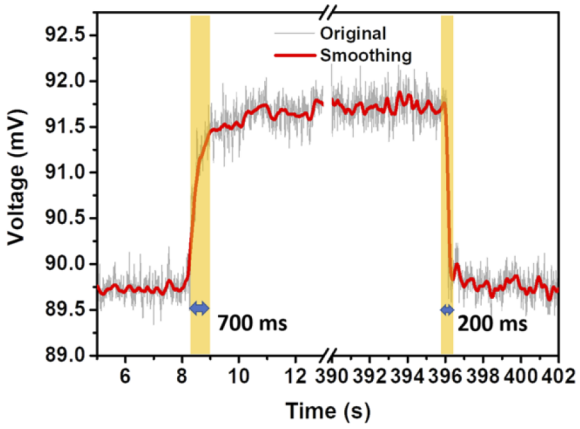

Fig. 9. Time response of MDA-WGM for the input laser power from 0 to 10.4 mW, then to 0.

Finally, in Table 1 we carried out a comparison of performance for different photo-thermally induced WGM tuning schemes reported in literature to date with the results of this work. It should be noted that in some cases direct comparison of sensitivities for the different schemes is not straightforward (e.g., in the case of lateral laser pumping). As can be seen from the table, the proposed scheme offers sensitivity second only to that of the MNPs embedded silica microsphere resonator, reported in [32]. However, the proposed scheme shows the highest sensitivity among the tunable WGM resonators operating under pump wavelengths shorter than 1550 nm. Since the MNPs have a smaller absorption coefficient at 980 nm, this suggests that the sensitivity for the proposed scheme could be significantly improved at 1550 nm. The tuning performance of the proposed scheme at different pump wavelengths will be reported in the near future.

Table 1. Comparison of different photo-thermal WGM tuning schemes

Type of sensor	Sensitivity	Pump wavelength	Tuning range
MNPs embedded silica microsphere resonator [32]	0.2 nm/mW	1550 nm	13 nm
MNPs infiltrated photonic crystal fiber resonator [17]	0.034 nm/mW	980 nm	3.6 nm
MNPs infiltrated capillary resonator based on injected laser pumping [16]	0.15 nm/mW	1527 nm	3.3 nm
MNPs infiltrated capillary resonator based on lateral laser pumping [33]	0.0382 nm/(mW · mm^{-2})	532 nm	0.15 nm
MNPs-coated microbottle resonator [34]	22 pm/mW	1550 nm	0.68 nm
Nematic LC infiltrated capillary resonator (this work)	**146.5 pm/mW**	**980 nm**	**3.28 nm**

4. Conclusion

In conclusion, a new thermo-optical tuning scheme has been proposed and experimentally demonstrated based on a cylindrical WGM resonator infiltrated with a nematic LC, where

Optics EXPRESS

the laser pump power is delivered through an MNPs coated fiber half-taper inserted into the capillary. Two types of the nematic liquid crystals (MLC-7012 and MDA-05-2782) were studied as the core materials for the capillary resonators (MLC-WGM and MDA-WGM). Experimentally demonstrated sensitivities for the MLC-WGM and MDA-WGM are 101.5 ± 3.5 pm/mW and 146.5 ± 3.5 pm/mW, with tuning ranges of 1.96 nm and 3.28 nm respectively. To investigate the influence of the MNPs coating on the resonator's response to pump power and temperature, similar experiment was carried out with an uncoated fiber half-taper. The result demonstrates that the temperature inside the capillary increases with the pump power increase, which in turn leads to the decrease of the effective RI of the capillary core and a red shift in the WGM resonances. Moreover, since the nematic LC is a birefringent medium, the temperature dependence of its extraordinary RI (n_e) is typically stronger than that of the ordinary RI (n_o) [35], which means that by achieving a certain type of the LC orientation within the microcapillary it should be possible to achieve a higher temperature (pump power) sensitivity of the WGM spectrum. The proposed tuning scheme offers the highest sensitivity among similar tunable WGM resonators operating at pump wavelengths of 980 nm or shorter. Since the MNPs have a higher absorption coefficient at 1550 nm, this suggests that the sensitivity for the proposed scheme could be significantly improved at 1550 nm. The high sensitivity of the proposed scheme makes it a promising candidate for future photonic devices, such as filters, optical switches and lasers.

Funding. Technological University Dublin (Fiosraigh Scholarship Award 2019); Department of Agriculture, Food and the Marine, Ireland (17/F/284).

Acknowledgments. Numerical simulation support was provided by Arun Kumar Mallik. Optical design support was provided by Fangfang Wei, Zhuochen Wang, and Anuradha Rout. Result analysis and manuscript revision supports were provided by Yuliya Semenova and Qiang Wu.

Disclosures. The authors declare no conflicts of interest.

Data availability. Data underlying the results presented in this paper are not publicly available at this time but may be obtained from the authors upon reasonable request.

References

1. M. S. Luchansky and R. C. Bailey, "High-Q optical sensors for chemical and biological analysis," Anal. Chem. **84**(2), 793–821 (2012).
2. A. Bozzola, S. Perotto, and F. De Angelis, "Hybrid plasmonic-photonic whispering gallery mode resonators for sensing: A critical review," Analyst **142**(6), 883–898 (2017).
3. A. E. Fomin, M. L. Gorodetsky, I. S. Grudinin, and V. S. Ilchenko, "Nonstationary nonlinear effects in optical microspheres," J. Opt. Soc. Am. B **22**(2), 459 (2005).
4. M. Mur, J. A. Sofi, I. Kvasić, A. Mertelj, D. Lisjak, V. Niranjan, I. Muševič, and S. Dhara, "Magnetic-field tuning of whispering gallery mode lasing from ferromagnetic nematic liquid crystal microdroplets," Opt. Express **25**(2), 1073 (2017).
5. F. Monifi, Ş. Kaya Özdemir, and L. Yang, "Tunable add-drop filter using an active whispering gallery mode microcavity," Appl. Phys. Lett. **103**(18), 181103 (2013).
6. A. Mahmood, V. Kavungal, S. S. Ahmed, G. Farrell, and Y. Semenova, "Magnetic-field sensor based on whispering-gallery modes in a photonic crystal fiber infiltrated with magnetic fluid," Opt. Lett. **40**(21), 4983 (2015).
7. V. Kavungal, G. Farrell, Q. Wu, A. K. Mallik, and Y. Semenova, "Thermo-optic tuning of a packaged whispering gallery mode resonator filled with nematic liquid crystal," Opt. Express **26**(7), 8431 (2018).
8. F. Vollmer, S. Arnold, and D. Keng, "Single virus detection from the reactive shift of a whispering-gallery mode," Proc. Natl. Acad. Sci. U. S. A. **105**(52), 20701–20704 (2008).
9. M. D. Baaske, M. R. Foreman, and F. Vollmer, "Single-molecule nucleic acid interactions monitored on a label-free microcavity biosensor platform," Nat. Nanotechnol. **9**(11), 933–939 (2014).
10. V. R. Dantham, S. Holler, C. Barbre, D. Keng, V. Kolchenko, and S. Arnold, "Label-free detection of single protein using a nanoplasmonic-photonic hybrid microcavity," Nano Lett. **13**(7), 3347–3351 (2013).
11. A. K. Mallik, G. Farrell, D. Liu, V. Kavungal, Q. Wu, and Y. Semenova, "A Coated Spherical Microresonator for Measurement of Water Vapor Concentration at PPM Levels in Very Low Humidity Environments," J. Light. Technol. **36**(13), 2667–2674 (2018).
12. G. Gardosi, B. J. Mangan, G. S. Puc, and M. Sumetsky, "Photonic Microresonators Created by Slow Optical Cooking," ACS Photonics **8**(2), 436–442 (2021).
13. N. Bavili, T. Balkan, B. Morova, M. Eryürek, Y. Uysallı, S. Kaya, and A. Kiraz, "Highly sensitive optical sensor for hydrogen gas based on a polymer microcylinder ring resonator," Sensors Actuators, B Chem. **310**(October 2019), 127806 (2020).

Optics EXPRESS

14. A. Tamada, Y. Ota, K. Kuruma, K. Watanabe, S. Iwamoto, and Y. Arakawa, "Single Plasmon Generation in an InAs/GaAs Quantum Dot in a Transfer-Printed Plasmonic Microring Resonator," ACS Photonics **6**(5), 1106–1110 (2019).
15. S. Zhu, L. Shi, B. Xiao, X. Zhang, and X. Fan, "All-Optical Tunable Microlaser Based on an Ultrahigh- Q Erbium-Doped Hybrid Microbottle Cavity," ACS Photonics **5**(9), 3794–3800 (2018).
16. Y. Liu, L. Shi, X. Xu, P. Zhao, Z. Wang, S. Pu, and X. Zhang, "All-optical tuning of a magnetic-fluid-filled optofluidic ring resonator," Lab Chip **14**(16), 3004–3010 (2014).
17. W. Lin, H. Zhang, B. Liu, B. Song, Y. Li, C. Yang, and Y. Liu, "Laser-tuned whispering gallery modes in a solid-core microstructured optical fibre integrated with magnetic fluids," Sci. Rep. **5**(July), 1–10 (2015).
18. M. Schadt, "Liquid crystal materials and liquid crystal displays," Annu. Rev. Mater. Sci. **27**(1), 305–379 (1997).
19. A. Safrani, "Spectropolarimetric method for optic axis, retardation, and birefringence dispersion measurement," Opt. Eng. **48**(5), 053601 (2009).
20. W. Beam, S. Using, F. L. Slm, C. J. Henderson, D. G. Leyva, and T. D. Wilkinson, "Free Space Adaptive Optical Interconnect at," Journal of Lightwave Technology **24**(5), 1989–1997 (2006).
21. Y. Lu, Y. Yang, Y. Wang, L. Wang, J. Ma, L. Zhang, W. Sun, and Y. Liu, "Tunable liquid-crystal microshell-laser based on whispering-gallery modes and photonic band-gap mode lasing," Opt. Express **26**(3), 3277 (2018).
22. P. F. McManamon, P. J. Bos, M. J. Escuti, J. Heikenfeld, S. Serati, H. Xie, and E. A. Watson, "A review of phased array steering for narrow-band electrooptical systems," Proc. IEEE **97**(6), 1078–1096 (2009).
23. Y. Wang, H. Li, L. Zhao, Y. Liu, S. Liu, and J. Yang, "Tapered optical fiber waveguide coupling to whispering gallery modes of liquid crystal microdroplet for thermal sensing application," Opt. Express **25**(2), 918 (2017).
24. M. Humar, M. Ravnik, S. Pajk, and I. Muševič, "Electrically tunable liquid crystal optical microresonators," Nat. Photonics **3**(10), 595–600 (2009).
25. A. K. Mallik, D. Liu, V. Kavungal, Q. Wu, G. Farrell, and Y. Semenova, "Agarose coated spherical micro resonator for humidity measurements," Opt. Express **24**(19), 21216 (2016).
26. A. Meldrum and F. Marsiglio, "Capillary-Type Microfluidic Sensors Based on Optical Whispering Gallery Mode Resonances," Rev. Nanosci. Nanotechnol. **3**(3), 193–209 (2014).
27. J. Li and S. T. Wu, "Two-coefficient Cauchy model for low birefringence liquid crystals," J. Appl. Phys. **96**(1), 170–174 (2004).
28. J. D. Suter, I. M. White, H. Zhu, and X. Fan, "Thermal characterization of liquid core optical ring resonators," IEEE/LEOS Int. Conf. Opt. MEMS Their Appl. Conf. 2006 **46**(3), 177–178 (2006).
29. G. Ghosh, "Temperature Dispersion of Refractive Indexes in Some Silicate Fiber Glasses," IEEE Photonics Technol. Lett. **6**(3), 431–433 (1994).
30. S. Mathews, G. Farrell, and Y. Semenova, "Liquid crystal infiltrated photonic crystal fibers for electric field intensity measurements," Appl. Opt. **50**(17), 2628–2635 (2011).
31. C. Bariáin, I. R. Matías, F. J. Arregui, and M. López-Amo, "Optical fiber humidity sensor based on a tapered fiber coated with agarose gel," Sensors Actuators B Chem. **69**(1), 127–131 (2000).
32. P. Zhao, L. Shi, Y. Liu, Z. Wang, S. Pu, and X. Zhang, "Iron-oxide nanoparticles embedded silica microsphere resonator exhibiting broadband all-optical wavelength tunability," Opt. Lett. **39**(13), 3845 (2014).
33. Y. Li, H. Zhang, B. Liu, J. Wu, B. Song, D. Yan, and C. Yang, "Tuning of whispering gallery modes in a magnetic-fluid-infiltrated silica capillary based on lateral pumping scheme," J. Opt. (United Kingdom) **19**(1), 015801 (2017).
34. R. Ma, S. Yuan, S. Zhu, L. Shi, and X. Zhang, "Tunable sub-kHz single-mode fiber laser based on a hybrid microbottle resonator," Opt. Lett. **43**(21), 5315 (2018).
35. J. Li, S. Gauza, and S. T. Wu, "Temperature effect on liquid crystal refractive indices," J. Appl. Phys. **96**(1), 19–24 (2004).